

# Warmer climate: less or more snow?

Jouni Räisänen

Received: 13 March 2007 / Accepted: 14 June 2007 / Published online: 12 July 2007  
© Springer-Verlag 2007

**Abstract** Changes in snow amount, as measured by the water equivalent of the snow pack (SWE), are studied using simulations of 21st century climate by 20 global climate models. Although the simulated warming makes snow season to shorten from its both ends in all of Eurasia and North America, SWE at the height of the winter generally increases in the coldest areas. Elsewhere, snow decreases throughout the winter. The average borderline between increasing and decreasing midwinter SWE coincides broadly with the  $-20^{\circ}\text{C}$  isotherm in late 20th century November–March mean temperature, although with some variability between different areas. On the colder side of this isotherm, an increase in total precipitation generally dominates over reduced fraction of solid precipitation and more efficient melting, and SWE therefore increases. On the warmer side, where the phase of winter precipitation and snowmelt are more sensitive to the simulated warming, the reverse happens. The strong temperature dependence of the simulated SWE changes suggests that projections of SWE change could be potentially improved by taking into account biases in simulated present-day winter temperatures. A probabilistic cross verification exercise supports this suggestion.

**Keywords** Climate change · Climate projection · Snow · Snow water equivalent · Snow depth

## 1 Introduction

Snow is an important part of the terrestrial climate system (Vavrus 2007). The presence of snow increases surface albedo, thereby cooling the Earth as a whole and particularly the Northern Hemisphere mid- to high-latitude continents. Snow also thermally isolates the atmosphere from the ground, thus lowering cold extremes of surface air temperature even more than the winter mean or the annual average temperature. By acting as a seasonal reservoir of water, snow likewise dramatically alters the hydrological cycle in midlatitudes and in the Arctic. Changes in the extent and amount of snow are therefore, of substantial interest in the context of anthropogenic climate change, both because of the feedbacks that they provide to changes in other aspects of climate and because of their impact on human societies and natural ecosystems (ACIA 2005).

Model simulations of greenhouse gas induced climate change in the Northern Hemisphere mid- to high-latitude continents indicate both a strong wintertime warming and an increase in winter precipitation (Meehl et al. 2007). An increase in precipitation, if acting alone, would lead to an increase in snowfall and consequently to increased amount of snow on ground. On the other hand, an increase in temperature will act to reduce the fraction of precipitation that falls as snow and to increase the melting of snow. Whether snow will be actually reduced or increased depends on the balance between these competing processes.

In addition to the relative magnitude of precipitation and temperature changes, changes in snow conditions will most likely depend on present-day temperature climate. In a recent study, Hosaka et al. (2005) used a high-resolution (20 km) atmospheric model, forced by increased greenhouse gas concentrations and changes in sea surface conditions from an atmosphere-ocean general circulation

---

J. Räisänen (✉)  
Division of Atmospheric Sciences,  
Department of Physical Sciences,  
University of Helsinki, P.O. Box 64,  
Gustaf Hällströmin katu 2, 00014 Helsinki, Finland  
e-mail: jouni.raisanen@helsinki.fi

model (AOGCM) simulation, to simulate snow conditions in the late 21st century. They found that, although the water equivalent of the snow pack (SWE) was reduced in most regions and seasons, SWE increased from February to April in large parts of Siberia and northernmost North America. Some, but not all of these areas also experienced an increase in SWE in December, whereas, there were virtually no areas with increased SWE in October and June. A regional climate model simulation for North America (Christensen et al. 2007, Fig. 11.13) supports the robustness of these findings by showing an increase in March mean SWE in parts of Alaska and Arctic Canada, but a decrease further to the south.

As compared with model simulations of late 21st century climate, studies of observed climate changes are complicated by a lower signal-to-noise ratio: for many aspects of climate, the effects of increased greenhouse gas concentrations are still difficult to separate from natural variability. In their review, Lemke et al. (2007) find that, although the Northern Hemisphere snow extent has decreased during the past four decades particularly in spring and summer, regional trends in snow conditions have been variable. However, in mountain regions of both Europe and western North America, decreases in the length of the snow season and/or SWE have been most pronounced at relatively low elevations (Scherrer et al. 2004; Mote et al. 2005; Mote 2006). Higher up, where winters are colder, snow has decreased less or, in some areas, increased.

The behaviour found in these model- and observation-based studies is physically expected. Where climate is cold enough, midwinter temperatures will remain substantially below zero even after a moderate warming. Thus, at least in the middle of the winter, the phase of precipitation and snowmelt should be quite insensitive to temperature changes. Conversely, where winters are milder, even a modest warming will act to convert part of the snowfall to rainfall and increase the frequency and intensity of melting episodes. The probability that changes in SWE will be dominated by changes in total precipitation, rather than by the expected overall warming, is therefore, smaller in mild than in cold areas.

Physical reasoning, observations and existing model studies all give some guidance to how snow conditions are likely to be altered in the future. On the other hand, all aspects of simulated 21st century climate change vary, to a smaller or larger extent, between different models. A more quantitative view of the expected changes therefore, requires a more systematic analysis of model simulations than has been done this far.

In this study we document the changes in SWE in a state-of-the-art multi-model ensemble of AOGCM simulations of 21st century climate, using data from twenty models participating in the World Climate Research

Programme Third Coupled Model Intercomparison Project (CMIP3; see <http://www-pcmdi.llnl.gov>). As conjectured above and as is demonstrated here with a diagnostic analysis, changes in total precipitation, in the fraction of precipitation that falls as snow, and in the efficiency of melting all play important roles in explaining the simulated changes in SWE. The conjectured strong dependence of the SWE changes on the present-day temperature climate is also confirmed. One implication of this temperature-dependence is that biases in present-day winter temperature need to be kept firmly in mind when interpreting model-simulated changes in snow amount.

The data sets used in the study are described in “Section 2”. The following section briefly discusses the simulated SWE conditions in the late 20th century, thereby complementing a similar analysis recently made by Roesch (2006). Model-simulated changes in SWE and related quantities are described and the causes of the SWE changes are diagnosed in “Section 4”, with the main focus on the second half of the 21st century. The dependence of the simulated SWE changes on present-day winter temperature is studied in more detail in “Section 5”. A probabilistic cross-verification exercise is also made, to show that methods that take into account biases in simulated winter temperatures might allow for more realistic projections of SWE change than are obtained by a direct use of model results. The main conclusions are given in “Section 6”.

## 2 Data sets

### 2.1 Model simulations

Twenty models participating in CMIP3 are selected (Table 1), that is, all models that provided simulations for the Special Report on Emissions Scenarios (Nakićenović and Swart 2000) A1B scenario and for which SWE was available in the database. Although some of the models—particularly CGCM3.1 (T47) and (T63), GFDL-CM2.0 and 2.1, GISS-EH and ER, and MIROC3 (hires) and (medres) are closely related with each other, all twenty models are retained here since substantial differences in climate change occasionally occur even between models with a seemingly similar formulation. For each model, 150 year (1950–2099) monthly time series of SWE and other climate parameters are formed by combining “20th Century Climate in Coupled Climate Models” (20C3M) simulations with 21st century simulations based on the A1B scenario. The details of the forcing vary with model, but all models include at least the increase in major anthropogenic greenhouse gases and some representation of anthropogenic aerosols in both the 20C3M and A1B simulations. Further details are given at <http://www-pcmdi.llnl.gov> and in Randall et al. (2007).

**Table 1** The models used in this study

Model	Institution
CCSM3	National Center for Atmospheric Research, USA
CGCM3.1 (T47)	Canadian Centre for Climate Modelling and Analysis
CGCM3.1 (T63)	Same as previous
CNRM-CM3	Météo-France
CSIRO-MK3.0	CSIRO Atmospheric Research, Australia
ECHAM5/MPI-OM	Max Planck Institute for Meteorology, Germany
ECHO-G	University of Bonn and Model & Data Group, Germany; Korean Meteorological Agency
FGOALS-g1.0	Chinese Academy of Sciences
GFDL-CM2.0	Geophysical Fluid Dynamics Laboratory, USA
GFDL-CM2.1	Same as previous
GISS-AOM	Goddard Institute for Space Studies, USA
GISS-EH	Same as previous
GISS-ER	Same as previous
INM-CM3.0	Institute for Numerical Mathematics, Russia
IPSL-CM4	Institut Pierre Simon Laplace, France
MIROC3.2 (hires)	Center for Climate System Research, National Institute for Environmental Studies and Frontier Research Center for Global Change, Japan
MIROC3.2 (medres)	Same as previous
MRI-CGCM2.3.2	Meteorological Research Institute, Japan
UKMO-HadCM3	Hadley Centre for Climate Prediction and Research/Met Office, UK
UKMO-HadGEM	Same as previous

Although parallel simulations started from different initial conditions are available for many of the models, only one simulation per model is used in this study. To ensure that the analysis is not unduly affected by internal variability, 50-year means of SWE and other variables are calculated for three periods: late 20th century (1950–1999, abbreviated as L20C), early 21st century (2000–2049, E21C) and late 21st century (2050–2099, L21C). The focus is mainly on a comparison of L21C with L20C, but some results are also shown for E21C. The analysis is conducted in a common  $2.5^\circ \times 2.5^\circ$  latitude–longitude grid, which is representative of the typical resolution of the models. The regridding from the original model grids to the analysis grid is made with the nearest-point method, to avoid, in particular, the mixing of land and sea points that would result from commonly used bilinear interpolation.

The focus in this study is on seasonally snow-covered Northern Hemisphere land areas. In each grid box, models with substantial August mean SWE (mean value over the years 1950–2099 above 10 mm) are excluded, to avoid the ensemble statistics from being contaminated by models with ongoing glaciation. The maps and statistics in this paper exclude all grid boxes in which 11 or more of the 20 models are eliminated based on this condition. Similarly excluded are grid boxes, which are snow-free over the whole period 1950–2099 in at least 11 of the 20 models.

## 2.2 Observational data sets

In “[Section 3](#)” below, some comparison is made between the simulated L20C SWE climatologies and SWE estimates from the Former Soviet Union Hydrological Snow Surveys (FSUHSS) data set (Krenke 1998), which is based on observations made at 1,345 sites throughout the former Soviet Union between 1966 and 1990. For this study, we used SWE route measurements carried out in the (open or forested, depending on site) terrain surrounding the observation stations. Each recorded value is a mean of ten SWE measurements along the route. The measurements were generally made on the 10th, 20th, and the last day of each month. To obtain unbiased mid-month values for comparison with the model-simulated monthly means, the 10th and 20th day measurements were averaged in this study. Many of the stations were operative for only a part of the period 1966–1990. Only stations with at least 15 years of data are used here. The data were gridded to the  $2.5^\circ \times 2.5^\circ$  analysis grid simply by selecting for each grid box the station with the longest time series. Altogether, data were available for 332 land grid boxes, with a good coverage in the southern but significantly worse coverage in the northeastern parts of the former Soviet Union.

For the evaluation of model-simulated surface air temperatures in “[Section 3](#)” and [Section 5](#), the University of

East Anglia Climate Research Unit (CRU) TS 2.1 data set (Mitchell and Jones 2005) was used. This data set is based on objective interpolation of station observations, and it has a resolution of  $0.5^\circ$  in both horizontal directions. For comparison with the model simulations, the CRU temperatures were averaged over the  $2.5^\circ \times 2.5^\circ$  grid boxes.

### 3 Simulated SWE climate in the late 20th century

Figure 1a shows the twenty-model, 1950–1999 mean SWE in March, when SWE is close to its seasonal maximum in northern North America and northern Eurasia. There is a general increase in SWE from milder midlatitude areas to colder high-latitude regions, but the inner parts of eastern Siberia with extremely cold and therefore, dry winters show up as an area with a relatively thin snow pack. Local

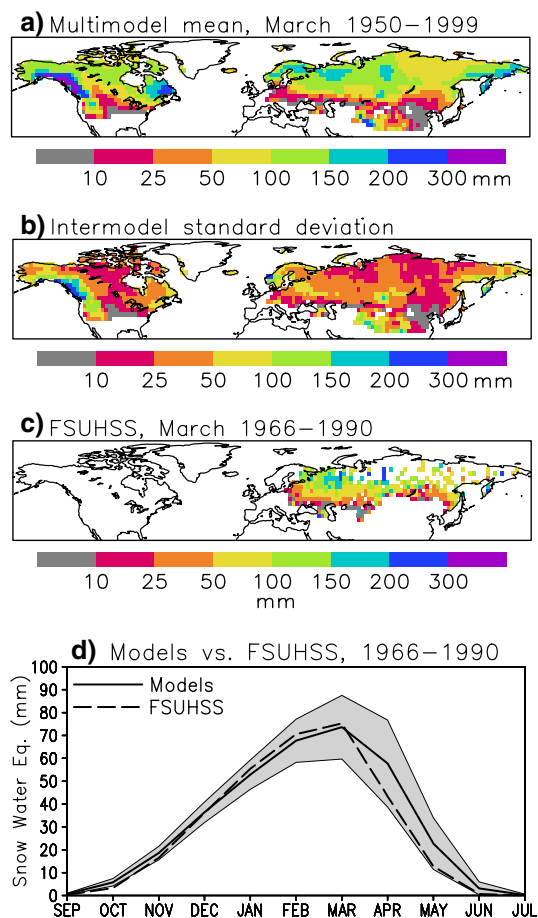


**Fig. 1** Snow climatology in the late 20th century. **a** March mean SWE in the years 1950–1999 as averaged over the 20 models; **b** intermodel standard deviation of March mean SWE; **c** March mean SWE in 1966–1990 from the FSUHSS data set; **d** area mean seasonal cycle of SWE in the models (*solid line* for the multi-model mean and shading for mean  $\pm$  one standard deviation) and from the FSUHSS data

maxima occur in the northern Rocky Mountains, where precipitation is enhanced by orographic forcing and in the eastern Labrador peninsula near the western end of the North Atlantic storm track. The intermodel standard deviation (Fig. 1b) is also generally largest in mountainous areas. However, in contrast with the multi-model mean SWE, there is little systematic north-south gradient in the standard deviation. Thus, the ratio between the standard deviation and the mean decreases northward, from around unity near the southern edge of the snow-covered area to less than 0.2 in parts of northern Eurasia and Arctic Canada (not shown).

Roesch (2006) recently compared SWE in 15 of the CMIP3 models with SWE estimates derived from the US Air Force Environmental Technical Application Center (USAF/ETAC) data set (Foster and Davy 1988), but he only showed results for continental scale mean values. To allow a more detailed comparison over the Former Soviet Union, the FSUHSS-based SWE estimate is given in Fig. 1c. This estimate is in general agreement with the model simulations. It shows larger variability on small geographical scales, but given that these data come from single stations and thus do not represent true grid box ( $2.5^\circ \times 2.5^\circ$ ) means this difference is unsurprising. Taking into account the difference in scale, the spatial correlation between the multi-model mean and the FSUHSS SWE estimate (0.71) is encouraging.

Figure 1d illustrates the seasonal cycle of SWE in the models and in the FSUHSS data set. Here the geographical averaging is done over the area covered by the FSUHSS data, and the time means for the models are calculated for the same period for which observations are available (however, the choice of the period makes little difference to the results). The agreement between the models and the FSUHSS data is good particularly from November to March, but most (although not all) models overestimate SWE in October and more markedly from April to June. The good agreement in the middle of the winter is somewhat at variance with Roesch (2006). He found almost all of the models to overestimate SWE in Eurasia in this season when compared with the USAF/ETAC data set, although he also noted that sparse measurements in mountainous areas might bias the USAF/ETAC estimates too low. However, his conclusion on too slow snowmelt in the models in spring agrees well with the present results. Another feature to be noted in Fig. 1d is the increase in intermodel variation towards the spring. The intermodel standard deviation in the area mean SWE is almost thrice as large in April as in January, although the multi-model mean SWE is almost the same in these two months.

The slow melting of the snow pack in spring coincides with a cold bias in the simulated temperatures in this season: the multi-model mean temperature over the area

covered by the FSUHSS data is 3°C below the CRU estimate in April, and almost 2°C below the CRU estimate in March and May. A cold bias of about 1.5°C is also found in the autumn, which may help to explain the somewhat too rapid growth of the simulated SWE in the beginning of the snow season. However, as noted by Roesch (2006), the cause-effect relationship is not necessarily simple. The cold bias itself might be amplified by the excessive snow cover particularly in spring when solar radiation is already abundant.

#### 4 Changes in SWE: a multi-model mean view

We now turn to the simulated future changes in SWE and related variables, using the simulations made for the SRES A1B emissions scenario. The focus in this section is on a documentation and diagnostic analysis of the multi-model mean changes. The uncertainty in the SWE projections implied by the variation between the individual models will be studied in “Section 5”.

The projected increase in greenhouse gas concentrations leads to a pronounced warming in most parts of the world, and particularly in the Northern Hemisphere mid- to high-latitude continents in winter. The simulated multi-model mean increase in the extended winter (November–March; NDJFM) mean temperature from L20C (1950–1999) to L21C (2050–2099) in Eurasia and North America is 3–7°C, with the largest warming in the northernmost parts (Fig. 2a). Precipitation also increases in the simulations, with the largest relative increase in the north (Fig. 2b). This increase in total precipitation translates into a general increase in NDJFM snowfall in northern North America and in the northern and eastern parts of Eurasia, where most winter precipitation is simulated to fall as snow even in the warmer L21C climate (Fig. 2c). The largest increases in northern Siberia exceed 45%, being very similar to the change in total precipitation. Further south and southwest over both Eurasia and North America, where winters are milder, NDJFM snowfall decreases. In these areas, there is a substantial decrease in the fraction of precipitation that falls as snow. This overcomes the increase in total precipitation, which by itself is smaller here than further north.

The relative change in SWE in March is shown in Fig. 2d. SWE increases in northernmost North America and much of Siberia, but the increase is limited to a smaller area than that in NDJFM snowfall. More generally, the percent change in March mean SWE is systematically more negative or less positive than the change in NDJFM snowfall. As will be illustrated later in this section, two factors contribute to this difference. First, even where the NDJFM snowfall increases, snowfall is reduced earlier in the autumn. Second, with the exception of the very coldest

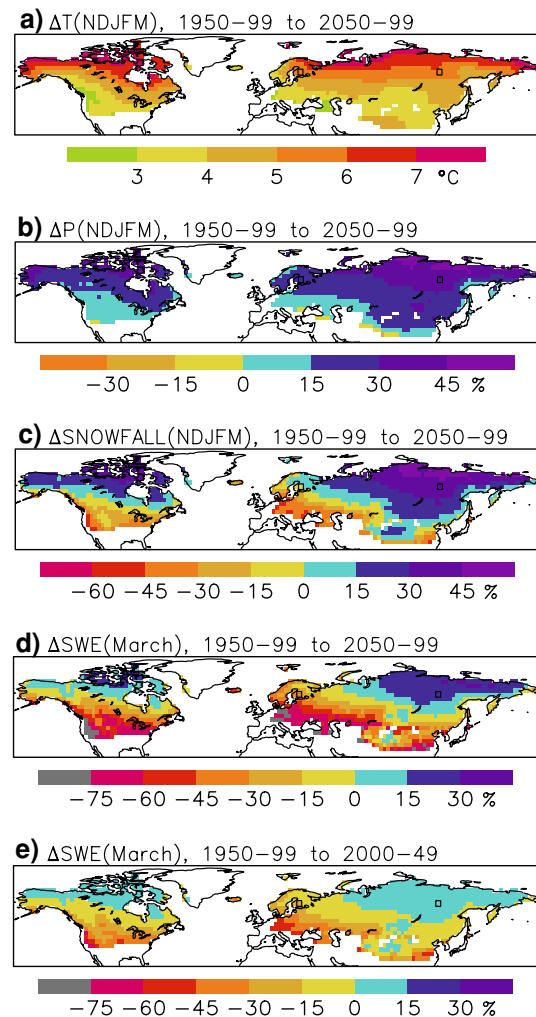


**Fig. 2** Simulated 20-model mean climate changes under the A1B scenario. **a–c**: extended winter (November–March) mean temperature, total precipitation and snowfall changes from 1950–1999 to 2050–2099; **d–e**: changes in March mean snow water equivalent from 1950–1999 to 2050–2099 and from 1950–1999 to 2000–2049. Grid boxes where less than 10 of the 20 models have snow or at least 11 models have perennial snow cover are masked out. The two grid boxes used in Fig. 3 are shown with *open squares*

areas, a larger fraction of the accumulated snowfall melts away before March in the simulated warmer climate.

The general features of change shown by Fig. 2b–d are very similar to those found by Hosaka et al. (2005) in their 20 km-resolution atmospheric model. The relatively coarse resolution of current AOGCMs is thus unlikely to be a major limitation for making projections of snow conditions on broad geographical scales, even though this conclusion is unlikely to hold for more localized projections in areas with complex topography.

The changes in March mean SWE from 1950–1999 to 2000–2049 (Fig. 2e) are smaller in magnitude than the changes to 2050–2099 (Fig. 2d), but the patterns of change

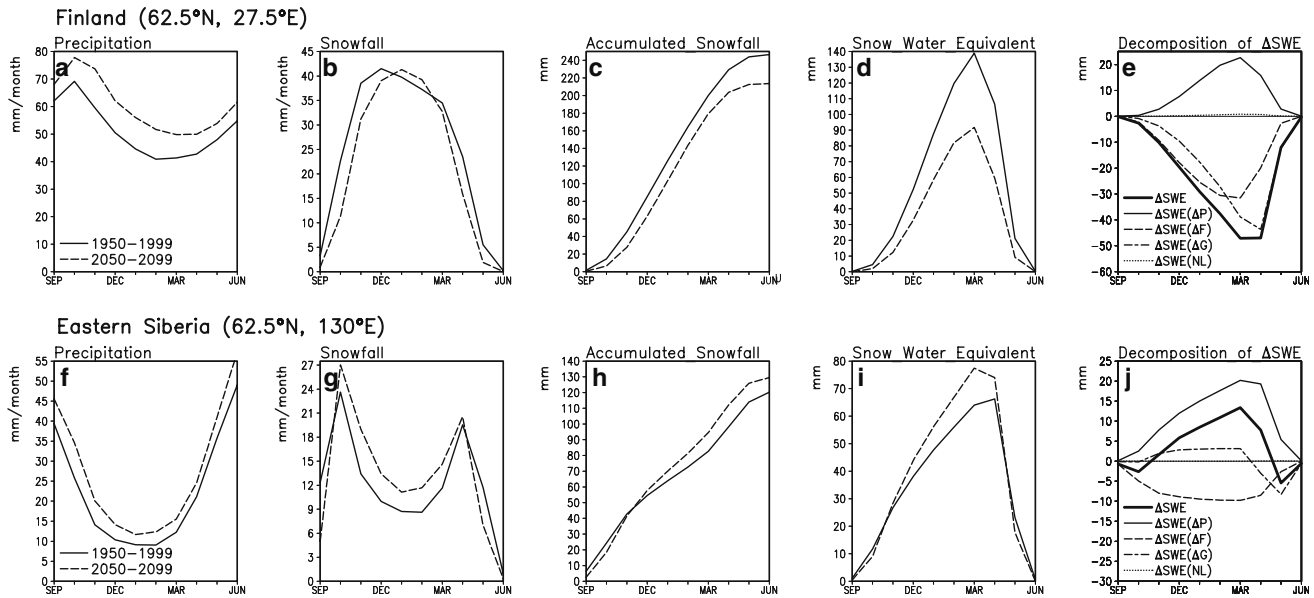


**Fig. 3** First four columns: comparison between 20-model mean L20C (1950–1999; *solid lines*) and L21C (2050–2099; *dashed lines*) climates in two grid boxes. From left to right: monthly mean precipitation and snowfall, accumulated snowfall from the beginning

of the winter, and monthly mean SWE. Fifth column: changes in SWE decomposed with Eq. [2]. See the legend for the identification of the individual terms

including the borderline between increasing and decreasing SWE are remarkably similar. With the caveat that Fig. 2 represents a multi-model mean view that smooths out the differences between individual models and the effects of internal variability, this suggests a fairly linear time evolution of snow conditions during this century.

As suggested above, three factors affect the changes in SWE: changes in (i) total precipitation, in (ii) the fraction of precipitation that falls as snow, and in (iii) the fraction of accumulated snowfall that has not melted away. To study the importance of these factors in more quantitative terms, the changes in SWE were diagnostically decomposed as follows. First, SWE was written as

$$SWE = G \int FP dt \tag{1}$$

where  $P$  denotes total precipitation,  $F$  the fraction of precipitation that falls as snow and  $G$  the fraction of accumulated snowfall that remains on the ground. The time integral was evaluated from August to the month considered; however, because the archived SWE data represent monthly means rather than end-of-month values, half-weight was given to the last month. Thus, the integral that corresponds to SWE in March was computed by summing the simulated snowfall ( $FP$ ) from August to February with half of the snowfall in March.

Let  $X$  represent any of SWE,  $G$ ,  $F$  and  $P$ , with  $X_{L20C}$  and  $X_{L21C}$  denoting the means of  $X$  in 1950–1999 and

2050–2099, respectively. By further introducing the notations  $\bar{X} = (X_{L20C} + X_{L21C})/2$  and  $\Delta X = (X_{L21C} - X_{L20C})$  one obtains

$$\begin{aligned} \Delta SWE = & \underbrace{\bar{G} \int \bar{F} \Delta P dt}_{\Delta SWE(\Delta P)} + \underbrace{\bar{G} \int \Delta F \bar{P} dt}_{\Delta SWE(\Delta F)} + \underbrace{\Delta G \int \bar{F} \bar{P} dt}_{\Delta SWE(\Delta G)} \\ & + \underbrace{\frac{1}{4} \Delta G \int \Delta F \Delta P dt}_{\Delta SWE(NL)} \end{aligned} \tag{2}$$

Thus, the difference between the L21C and L20C values of SWE is divided into four parts. The first of these represents changes in total precipitation, the second the changes in the fraction of precipitation that falls as snow, and the third the changes in the fraction of accumulated snowfall that remains on the ground at a given time of the year. The fourth, nonlinear (NL) term involves a combination of the changes in all of  $G$ ,  $F$  and  $P$ . This term is typically at least an order of magnitude smaller than the first three.

Equation [2] was applied separately to each model. Here, however, only the 20-model means of the resulting decomposition are discussed. Figure 3 illustrates the results for two grid boxes in northern Eurasia, one in Finland (62.5°N, 27.5°E) and the other near Yakutsk in eastern Siberia (62.5°N, 130°E), which are both marked with open squares in Figs. 2, 4. Although located at the same latitude, these two points have very different winter climates. The

grid box in Finland represents a relatively mild semi-maritime climate influenced by predominantly westerly winds from the Atlantic Ocean, whereas the one in eastern Siberia has a highly continental climate with extremely cold winters. The 20-model mean NDJFM mean temperature in 1950–1999 in the grid point in Finland is  $-12.7^{\circ}\text{C}$ , that in the point in eastern Siberia  $-31.5^{\circ}\text{C}$ . The difference in the real world is even larger: the corresponding CRU temperature estimates for the two points are  $-6.4$  and  $-34.2^{\circ}\text{C}$ , respectively. The implications that biases in present-day temperatures may have on the interpretation of the simulated SWE changes will be studied in “Section 5”.

In Finland the 20-model mean SWE is reduced from L20C to L21C throughout the winter, but in eastern Siberia it increases, with the exception of the beginning (October) and end (May) of the snow season (see the fourth column and the thick lines for  $\Delta\text{SWE}$  in the fifth column of Fig. 3). The factors that contribute to this contrasting behaviour are addressed below.

In both two grid boxes, the simulated 20-model mean total precipitation (Fig. 3a, f) increases in all months from September to June. If this increase in precipitation were acting alone, SWE would also have increased in Finland, and the increase in SWE in eastern Siberia would have been larger than actually simulated (see the lines for  $\Delta\text{SWE}(\Delta\text{P})$  in Fig. 3e, j).

In the simulated warmer future climate, a smaller fraction of precipitation in Finland falls as snow. Thus, although the total precipitation increases throughout the winter, snowfall only increases slightly in January and February and decreases in all other months (Fig. 3b). Because the increase in snowfall in January and February does not balance the decrease up to December, the accumulated snowfall ( $\int \text{FP} dt$  in (1)) in Finland is, for any part of the winter, smaller in 2050–2099 than in 1950–1999 (Fig. 3c).

The decomposition (2) identifies the decrease in the fraction of solid precipitation as the main cause of reduced SWE in Finland in autumn and early winter, until February (see the line for  $\Delta\text{SWE}(\Delta\text{F})$  in Fig. 3e). The same factor also moderates the increase in SWE in eastern Siberia (Fig. 3j). Here, the phase of precipitation is insensitive to the simulated warming during most of the extremely cold winter, and the increase in total precipitation therefore, also leads to an increase in snowfall (Fig. 3g). Early in the autumn (September) and late in the spring (May), however, the situation is different. The shift between mostly liquid and mostly solid precipitation occurs later in the autumn and earlier in the spring, and snowfall therefore, decreases although total precipitation increases.

The second main cause of the simulated decrease in SWE in Finland is a decrease in the fraction of the accumulated snowfall that remains on the ground, or, conversely, an increase in the fraction of accumulated snowfall that has

melted away. The decomposition (2) identifies  $\Delta\text{SWE}(\Delta\text{G})$  as the main contributor to reduced SWE in Finland beginning from March (Fig. 3e), and the same term also explains the slight decrease in SWE in eastern Siberia late in the spring (Fig. 3j). Earlier in the winter, however, this term is slightly positive in eastern Siberia. In interpreting this apparently surprising result, it is essential to note that this term represents the change in the *fraction* of accumulated snowfall that remains on the ground, not the absolute change in snowmelt. Beginning from December, the simulated accumulated snowfall in eastern Siberia is larger in 2050–2099 than in 1950–1999 (Fig. 3h). As there is little change in the absolute amount of snowmelt, the fraction of accumulated snowfall that remains on the ground grows slightly larger. Thus, although  $\Delta\text{G}$  in (2) primarily responds to changes in temperature, it is also to some extent affected by changes in precipitation.

Finally, the nonlinear term  $\Delta\text{SWE}(\text{NL})$  in Eq. (2) is very small, both in the grid boxes used in Fig. 3 (see the dotted lines in the last column) and elsewhere. It is therefore, excluded from further discussion.

The simulated 2050–2099 minus 1950–1999 changes in March mean SWE are decomposed with (2) in Fig. 4. The first map duplicates Fig. 2d, except for giving the SWE changes in absolute rather than relative units. The changes in total precipitation and in the fraction of solid precipitation have competing effects, the former acting to increase and the latter to decrease SWE (Fig. 4b, c). However, the contribution from increased precipitation (Fig. 4b) increases towards north. This is partly because the increase in winter precipitation is percentwise largest in high latitudes (Fig. 2b), but also because a larger fraction of the precipitation falls as snow and a larger fraction of the snowfall remains on the ground in cold climates. Disregarding the small nonlinear term, the first two right-hand-side terms in (2) sum up to give the SWE change attributable to changes in accumulated snowfall (Fig. 4d). Mostly because of the north–south gradient seen in Fig. 4b, this sum is positive in Alaska, northern Canada and the northeastern parts of Eurasia, but generally negative elsewhere. The pattern is similar to the change in NDJFM snowfall in Fig. 2c, but because (2) also counts in decreases in snowfall before November, positive values are slightly less extensive in Fig. 4d.

The SWE contribution attributed to changes in the fraction of accumulated snowfall that remains on the ground is slightly positive in eastern Siberia and northernmost Canada (Fig. 4e). As noted above, this is an indirect result of increased snowfall. Elsewhere, this term is negative, reflecting the increased efficiency of melting in a warmer climate. Particularly large negative values are seen in two belts that extend across midlatitude North America and from Scandinavia to western Russia. These belts are located in areas where the present-day climate is

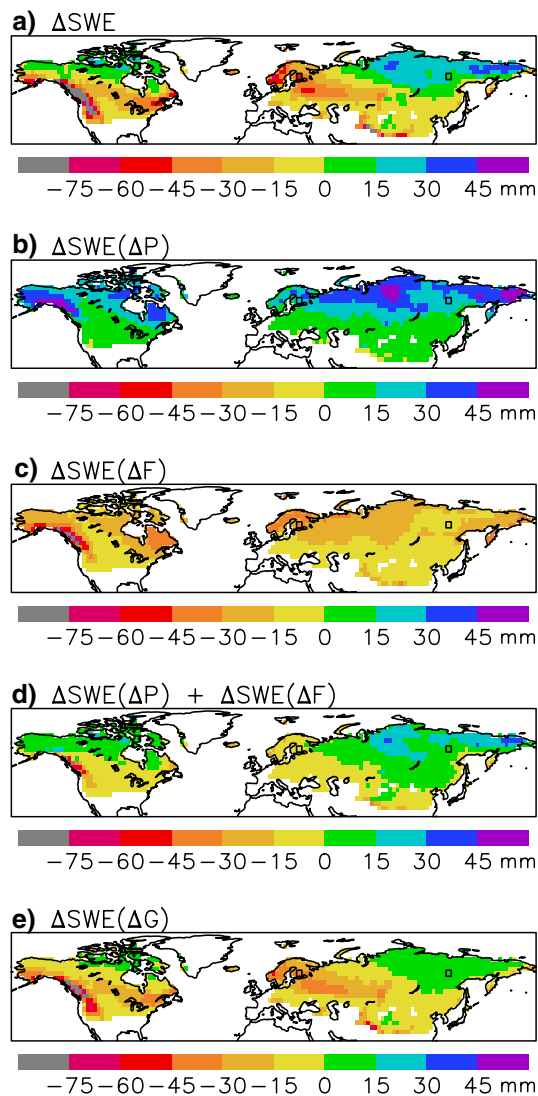


**Fig. 4** 20-model mean changes (2050–2099 minus 1950–1999) in March mean SWE (a), and their decomposition using Eq. [2]. Panels b and c show the contributions of precipitation change and the change in the fraction of solid precipitation, respectively. The sum of these terms, representing the total SWE contribution from changes in accumulated snowfall, is given in (d), and the contribution from changes in the fraction of accumulated snowfall remaining on the ground in (e). The two grid boxes used in Fig. 3 are shown with *open squares*

still cold enough to maintain a substantial snow pack in March, but where increased melting associated with an earlier onset of spring leads to a large decrease in SWE in a simulated warmer climate. Similar belts are seen in the total SWE change in Fig. 4a.

## 5 Changes in SWE: a probabilistic view

To give a simple illustration of the intermodel variation in the SWE projections, the top row of Fig. 5 shows for each

grid box the per cent fraction of models in which March mean SWE increases. In the coldest parts of Siberia and Arctic Canada, all models agree on an increase in SWE from 1950–1999 to 2050–2099 (Fig. 5a). Conversely, in large parts of the United States and midlatitude western Eurasia, SWE decreases in all models. Between these extremes, the models partially disagree, with some of them simulating increases and others decreases in SWE. The results for 2000–2049 (Fig. 5b) are similar to those for 2050–2099, but areas with perfect agreement are less extensive and areas with a near equal split between increases and decreases are more common. This reflects the lower signal-to-noise ratio during this earlier period, when greenhouse gas induced changes in SWE are more likely to be confounded by internal climate variability than later in the 21st century.

The general increase in SWE in the coldest parts of Eurasia and North America and the general decrease in SWE in milder areas together suggest a strong relationship between the simulated SWE changes and present-day winter temperature. A quantification of this physically expected relationship is given in Fig. 6. To generate this figure, the grid boxes in the seasonally snow-covered Northern Hemisphere continents were divided into six classes according to the simulated 1950–1999 NDJFM mean temperature with class boundaries at 5°C intervals from –25 to –5°C. Intermodel differences in present-day climate were taken into account by making the classification separately for each model. Then, for each class and model, the total areas of increasing and decreasing SWE were computed. Finally, by averaging these areas over the 20 models, the multi-model mean fractional area of increasing SWE was derived for each of the six temperature classes. For reference, the CRU analysis of the NDJFM mean temperature in 1950–1999 is given in Fig. 7a.

Fig. 6a shows that, in areas where the late 20th century NDJFM mean temperature exceeds –10°C, there is only very rarely more snow in 2050–2099 than in 1950–1999. Even within the class –15 to –10°C, increases in snow are uncommon, covering at maximum 25% of this area in February. Proceeding towards lower temperatures, the class –25 to –20°C is the first one with increases in SWE dominating at the height of the winter, from January to March. In the coldest class with NDJFM mean temperatures below –25°C, increases in SWE dominate strongly from December to April, with a maximum of over 90% in March. Even in this class, however, increases in SWE are uncommon early in the autumn and late in the spring. Thus, even in those areas where the simulations suggest an increase in SWE at the height of the winter, they indicate a shortening of the snow season from its both ends. This behaviour confirms the results of Hosaka et al. (2005) for a much wider range of simulations.



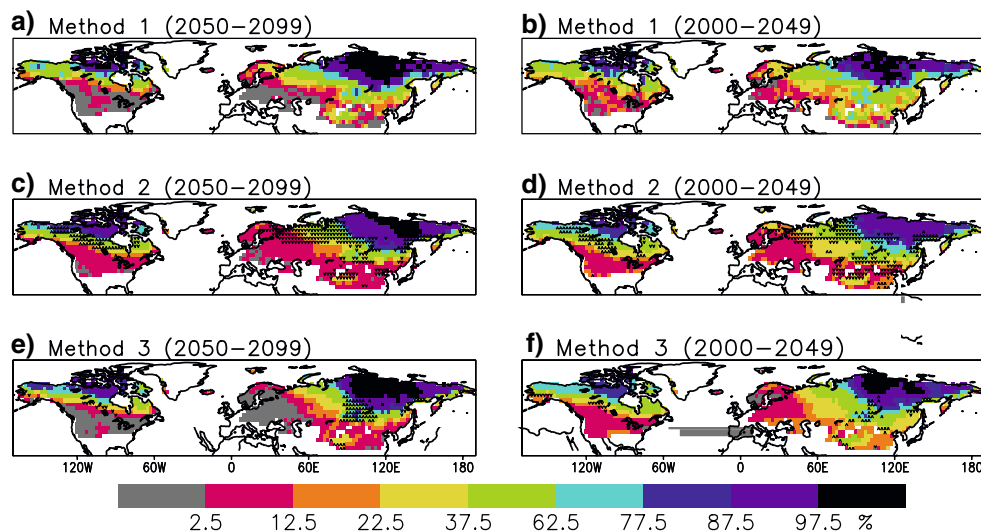
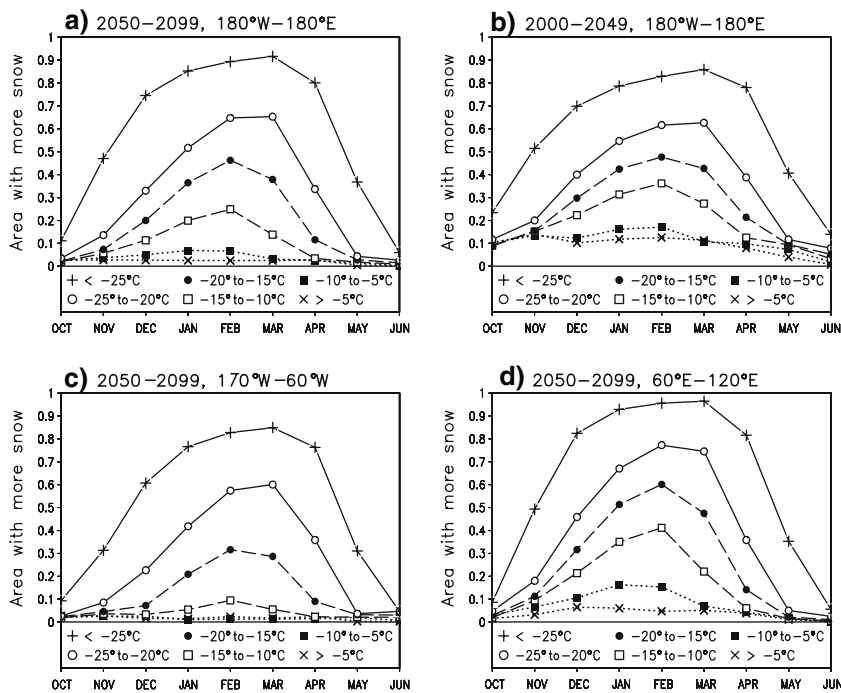


**Fig. 5** Probability of increasing March mean SWE relative to 1950–1999, as estimated from the 20-model ensemble with three methods. **a–b** simple count of models; **c–d** probability inferred from observed NDJFM mean temperature and the model-simulated relationship between NDJFM mean temperature and future SWE changes; **e–f** hybrid method (see text). The left column represents the changes from 1950–1999 to 2050–2099 and the right column those to 2000–2049.

The *arrowheads* in **c–d** indicate grid boxes where the absolute difference between Method 2 and Method 1 exceeds 15%; *upward* (*downward*) pointing *arrowheads* are used where Method 2 gives a higher (lower) probability of SWE increase than Method 1. In the same manner, the *arrowheads* in **e–f** indicate grid boxes where the absolute difference between Method 3 and Method 2 exceeds 15%

**Fig. 6** Probability of increasing SWE as a function of the simulated 1950–1999 NDJFM mean temperature, as inferred from the 20-model ensemble. **a** changes from 1950–1999 to 2050–2099 and **b** changes from 1950–1999 to 2000–2049, including both North America and Eurasia. **c** as **a** but for North America only. **d** as **c** but for western and central Asia at longitudes 60°–120°E



The same analysis for the changes from 1950–1999 to 2000–2049 (Fig. 6b) yields qualitatively similar results but with a slightly weaker relationship between the temperature climate and the SWE change. Even where the 1950–1999 NDJFM mean temperature exceeds  $-5^{\circ}\text{C}$ , over 10% of the grid boxes show an increase in mid-winter SWE in

2000–2049. Conversely, even where the NDJFM temperature is below  $-25^{\circ}\text{C}$ , the models still suggest a 15% chance of decreasing SWE in March. The implication is that, in some areas, SWE changes in the early 21st century may still be dominated by internal variability, so that the direction of the changes during this period may not be

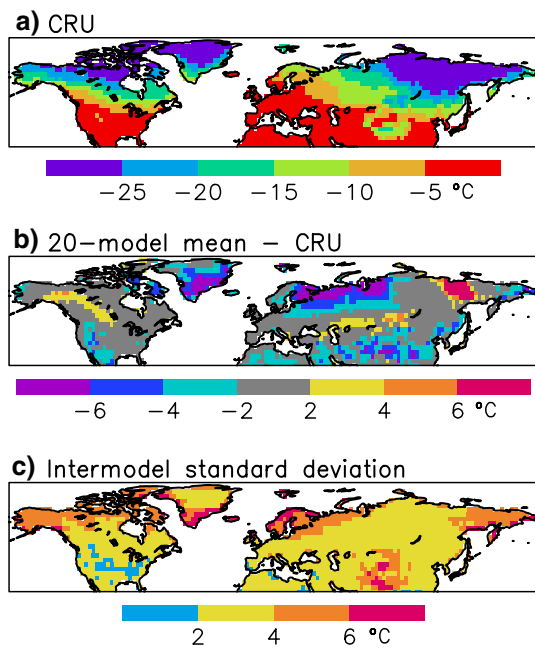


**Fig. 7** NDJFM mean temperature in 1950–1999. **a** CRU analysis; **b** 20-model mean minus CRU; **c** standard deviation between the models

representative of the long-term response to increasing greenhouse gas concentrations.

A closer analysis reveals that the relationship between the NDJFM mean temperature and the sign of the SWE changes has some geographical variability. This is illustrated in Fig. 6c–d, which repeat the analysis of Fig. 6a for two large subregions: North America, and western-to-central Asia covering the longitude range 60°–120°E. For each temperature class, increases in SWE are more common in the latter region. For example, within the class –15 to –10°C, the fraction of increasing SWE in February is only 10% in North America, but 40% in western-to-central Asia. The causes of this difference require further investigation. It does not appear to be explained in any simple way by the simulated temperature and precipitation changes, which are quite similar in the two regions.

The relationship between present-day winter temperatures and simulated SWE changes indicates that the interpretation of the latter needs to take into account biases in the simulated temperature climate. As shown by Fig. 7b, there are some areas where the multi-model mean simulated NDJFM temperatures differ substantially from the CRU observational estimate. For example, a cold bias of up to 6°C occurs in northwestern Eurasia, which suggests that the ensemble likely overestimates the chance of SWE increase in this area. On the other hand, the simulated temperatures vary between the individual models (Fig. 7c). This variation might partly explain the intermodel variation of the SWE changes.

The last two rows in Fig. 5 show two alternative estimates for the probability of March mean SWE increase, denoted as Method 2 and Method 3. Method 2 assumes that the probability of SWE increase is solely determined by the observed NDJFM mean temperature, and that the relationship between temperature and probability can be derived from the multi-model ensemble with the same principle that was used for generating Fig. 6. In this case, however, the non-overlapping 5°C temperature blocks of Fig. 6 were replaced by a 5°C window stepped with 1°C intervals. For example, the “observed” (i.e., CRU) L20C NDJFM temperature in the grid box studied in Fig. 3a–e was –6.4°C. For estimating the probability of SWE increase in this grid box, Method 2 thus used the SWE data from all grid boxes in which the simulated L20C NDJFM temperature was between –4 and –9°C. Again, the suitable grid boxes were selected for each model separately.

Method 2 accounts for biases in simulated temperature, but its assumption on a geographically invariant relationship between temperature and the sign of the SWE change appears to be overly simplified (Fig. 6c–d). Thus, a hybrid method was also developed (Method 3). This was otherwise similar to Method 2 but it only used grid boxes within 10° latitude and 10° longitude from the location for which the probability of SWE increase was being estimated. Taking again the Finnish grid box at (62.5°N, 27.5°E) as an example, the search for grid boxes with suitable temperatures was restricted to the area (52.5°–72.5°N, 17.5°–37.5°E).

On their largest scales, the three sets of maps in Fig. 5 are similar. Nevertheless, there are non-negligible differences in the details, particularly between Method 1 (directly model-based probabilities) and Method 2 (purely temperature-based probabilities). For example, in Scandinavia and northwestern Russia, where Fig. 7b reveals a cold bias in the models, Method 2 suggests a much smaller chance of SWE increase than Method 1. The differences between Methods 2 and 3 are more subtle. However, Method 3 suggests a larger probability of SWE increase than Method 2 in central Siberia, and a generally smaller probability of SWE increase in southern Canada (see the arrowheads in Fig. 5c–f for the largest differences between the three methods). In some areas, such as in mid-latitude North America especially in 2050–2099, the probability estimates from Method 3 are closer to Method 1 than those from Method 2 are. However, the reverse happens in other areas, most notably in northern Europe, where Method 3 suggests an even lower probability of SWE increase than Method 2.

The probability estimates in Fig. 5 are conditional to a particular forcing scenario. Method 1 additionally assumes that the uncertainty in modelling climate response to anthropogenic forcing is adequately represented by the variation within the multi-model ensemble, whereas Methods 2 and 3 require that the ensemble captures the

uncertainty in the relationship between climatological winter temperatures and future SWE changes. The extent to which the probabilities shown in Fig. 5 can be interpreted as probabilities of SWE change in the real world is therefore a complicated issue (see Allen and Ingram (2002) for further discussion). Nonetheless, probabilistic cross-verification (e.g., Räisänen and Ruokolainen 2006) can be used to study whether Methods 2 and 3, which attempt to eliminate the effect of temperature biases, should be preferred over the direct count of models in Method 1. In cross-verification, each model in turn is chosen as a pseudo-truth against which the probabilistic forecasts obtained from the other models are verified, and the resulting verification statistics are averaged over all choices of the verifying model. Better cross-verification statistics also suggest a potential improvement of forecasts for the real world, provided that the methodological improvement that benefited the cross-verification is not drowned by other sources of error.

A basic verification statistic for probability forecasts is the Brier score  $B$  (Brier 1950; Wilks 1995). Here we calculate  $B$  for the event  $E$  “the mean March SWE in 2050–2099 (or 2000–2049) exceeds that in 1950–1999”. As evaluated over  $N$  cases,

$$B = \sum_{i=1}^N m_i(p_i - o_i)^2 / \sum_{i=1}^N m_i \tag{3}$$

where  $o_i = 1$  (0) if  $E$  occurs (does not occur) in case  $i$  and  $p_i$  is the corresponding forecast probability.  $m_i$  is the weight given to case  $i$ ; here we weight grid boxes according to their area. For a perfect deterministic forecast system, which gives a probability of 1 (0) always when  $E$  occurs (does not occur),  $B = 0$ .

The resulting Brier scores, averaged over the 20 choices of the verifying model and over the seasonally snow-covered Northern Hemisphere continents as defined in “Section 2”, are given in Table 2. The score for Method 1 is much lower in 2050–2099 than in 2000–2049 because, in the late 21st century, the signal-to-noise ratio of the SWE changes is higher and areas with a near equal split between models with increasing and decreasing SWE are less common. The differences between the three methods are smaller but, in both periods, Method 2 beats Method 1. This suggests that the correction of temperature-related biases in Method 2 in fact has some value<sup>1</sup>. However, Method 2 is outperformed by Method 3, albeit only very

<sup>1</sup> Some decrease in  $B$  from Method 2 to Method 1 would be expected simply because the geographical averaging in Method 2 increases the sample size, but the differences shown in Table 2 are larger than can be explained by this factor alone (see Appendix in Räisänen and Ruokolainen 2006).

**Table 2** Average cross-verification Brier scores for the sign of the March mean SWE change from 1950–1999 to 2050–2099 and 2000–2049 for the three methods used in Figure 5

Forecast period	Method 1	Method 2	Method 3
2050–2099	0.1155	0.1005	0.0975
2000–2049	0.1641	0.1520	0.1516

slightly. This implies that the relationship between present-day winter temperature and SWE change in the CMIP3 ensemble has some genuine geographical variability, so that the differences between Fig. 5c–d and e–f are not explained by sampling effects alone. This conclusion is supported by similar analysis for other calendar months: in both two 50-year periods, Method 3 yields lower Brier scores than the other two methods in all months from November to May (not shown).

## 6 Conclusions

Model simulations of greenhouse gas induced climate change in the Northern Hemisphere mid- to high-latitude continents indicate both a substantial warming and an increase in winter precipitation. The increase in temperature acts to reduce the amount of snow both by reducing the fraction of precipitation that falls as snow and by increasing snowmelt, but the increase in precipitation acts to the opposite direction. Whether snow will be actually reduced or increased depends on the balance between these competing factors.

Here we have analysed simulations of snow amount, measured by the snow water equivalent (SWE), by twenty climate models participating in the Third Coupled Model Intercomparison Project (CMIP3). The main characteristics of simulated 21st century SWE change under the SRES A1B emissions scenario are the following:

1. At the height of the winter, SWE increases in the coldest parts of the Northern Hemisphere continents, such as northernmost North America and most of Siberia. Elsewhere, SWE decreases. The average borderline between increasing and decreasing SWE coincides broadly with the  $-20^{\circ}\text{C}$  isotherm in late 20th century extended winter (NDJFM) mean temperature. Although this temperature threshold is not abrupt and has some geographical variability, increases in SWE in the late 21st century occur only very rarely in grid boxes in which the NDJFM mean temperature exceeds  $-10^{\circ}\text{C}$ . Conversely, where the NDJFM mean temperature is below  $-25^{\circ}\text{C}$ , the models suggests a very large chance (up to 90% in March) of SWE increase.

2. Even where SWE increases at the height of the winter, it decreases early in the autumn and late in the spring. Thus, the snow season is shortened.
3. The characteristics of SWE change in the early 21st century are similar to those in the late 21st century, but the changes are smaller and their signal-to-noise ratio is therefore, lower. This results in a worse intermodel agreement on the sign of the SWE changes in the early than in the late 21st century.

A diagnostic analysis separates three factors that are all important for the simulated SWE changes. If acting alone, increased total precipitation would lead to increased SWE in nearly all snow-covered areas, but the increase would be largest in the northernmost parts where the snowfall season is longest and the relative increase in precipitation is largest. However, decreases in the fraction of solid precipitation reduce SWE in a warmer climate. This factor plays a role even in very cold areas, where nearly all precipitation remains solid in winter but the change between rain and snow occurs later in the autumn and earlier in the spring. Finally, more efficient melting in a warmer climate acts to reduce the fraction of accumulated snowfall that remains on the ground. This factor is the main contributor to reduced SWE in spring.

Systematic temperature biases in some areas such as northwestern Eurasia, together with the strong temperature dependence of the simulated SWE changes, indicate that the direct use of model output may not be the best way to derive projections of future SWE change. This idea is supported by a cross-verification analysis, which suggests that methods that account for temperature biases should permit potentially better probabilistic forecasts of, at least, the sign of the SWE change.

Based on an analysis of the physical mechanisms and on the agreement of the CMIP3 simulations between themselves and with earlier model studies, both the increase in SWE in the coldest parts of the Northern Hemisphere continents and the decrease in SWE in most midlatitude areas are likely to be robust features of greenhouse gas induced climate change. In between, where a more delicate balance between increased precipitation, decreased fraction of solid precipitation and more efficient melting results in a more equal split between models with increasing and decreasing SWE, the projections of SWE change are far more uncertain. In addition to the present-day temperature biases, there are at least two questions that need attention when assessing the likely direction of SWE changes in such areas. First, does the simulated SWE have the right sensitivity to temperature and precipitation changes? Second, is the ratio between precipitation and temperature changes correct in simulations of future climate? Some information on the first of these questions might be gained

by studying the characteristics of interannual climate variability. However, the second question might still be very hard to answer, because the signal-to-noise ratio of the observed 20th and early 21st century climate changes is probably not high enough for this purpose.

**Acknowledgments** We acknowledge the modeling groups for making their model output available as part of the WCRP's CMIP3 multi-model dataset, the Program for Climate Model Diagnosis and Intercomparison (PCMDI) for collecting and archiving this data, and the WCRP's Working Group on Coupled Modelling (WGCM) for organizing the model data analysis activity. The WCRP CMIP3 multi-model dataset is supported by the Office of Science, US Department of Energy. This paper benefited from the constructive comments of two anonymous reviewers.

## References

- ACIA (2005) Arctic climate impact assessment: scientific report. Cambridge University Press, London, p 1042
- Allen MR, Ingram WJ (2002) Constraints on future changes in climate and the hydrologic cycle. *Nature* 419:224–232
- Brier GW (1950) Verification of forecasts expressed in terms of probability. *Mon Wea Rev* 78:1–3
- Christensen JH, Hewitson B, Busuioc A, Chen A, Gao X, Held I, Jones R, Kwon W-T, Laprise R, Magaña Rueda V, Mearns L, Menéndez CG, Räisänen J, Rinke A, Kolli RK, Sarr A, Whetton P (2007) Regional climate projections. In: Solomon S et al (eds) *Climate change 2007: the physical science basis*. Cambridge University Press, London, pp 847–940
- Foster D, Davy R (1988) Global snow depth climatology. USAF Publ. USAFETAC/TN-88/006, Scott Air Force Base, Illinois, p 48
- Hosaka M, Nohara D, Kitoh A (2005) Changes in snow coverage and snow water equivalent due to global warming simulated by a 20 km-mesh global atmospheric model. *SOLA* 1:93–96
- Krenke A (1998) Former Soviet Union hydrological snow surveys, 1966–1996. Edited by NSIDC. National Snow and Ice Data Center/World Data Center for Glaciology, Digital media, Boulder
- Lemke P, Ren J, Alley R, Allison I, Carrasco J, Flato G, Fujii Y, Kaser G, Mote P, Thomas R, Zhang T (2007) Observations: changes in snow, ice and frozen ground. In: Solomon S et al (eds) *Climate change 2007: the physical science basis*. Cambridge University Press, London, pp 337–383
- Meehl GA, Stocker TF, Collins W, Friedlingstein P, Gaye A, Gregory J, Kitoh A, Knutti R, Murphy J, Noda A, Raper S, Wattersson I, Weaver A, Zhao Z-C (2007) Global climate projections. In: Solomon S et al (eds) *Climate change 2007: the physical science basis*. Cambridge University Press, London, pp 747–845
- Mitchell TD, Jones PD (2005) An improved method of constructing a database of monthly climate observations and associated high-resolution grids. *Int J Climatol* 25:693–712
- Mote PW (2006) Climate-driven variability in mountain snowpack in western North America. *J Clim* 19:6209–6220
- Mote PW, Hamlet AF, Clark MP, Lettenmaier DP (2005) Declining mountain snowpack in western North America. *Bull Am Meteor Soc* 86:39–49
- Nakićenović N, Swart R, Eds. (2000) *Emission Scenarios*. A special report of Working Group III of the Intergovernmental Panel on Climate Change. Cambridge University Press, London, p 599
- Räisänen J, Ruokolainen L (2006) Probabilistic forecasts of near-term climate change based on a resampling ensemble technique. *Tellus* 58A:461–472

- Randall DA, Wood RA, Bony S, Colman R, Fichefet T, Fyfe J, Kattsov V, Pitman A, Shukla J, Srinivasan J, Stouffer RJ, Sumi A, Taylor KE (2007) Climate models and their evaluation. In: Solomon S et al (eds) *Climate change 2007: the physical science basis*. Cambridge University Press, London, pp 589–662
- Roesch A (2006) Evaluation of surface albedo and snow cover in AR4 coupled climate models. *J Geophys Res* 111:D15111, doi:10.1029/2005JD006743
- Scherrer SC, Appenzeller C, Laternser M (2004) Trends in Swiss alpine snow days—the role of local and large-scale climate variability. *Geophys Res Lett* 31, doi:10.1029/2004GL020255
- Vavrus S (2007) The role of terrestrial snow cover in the climate system. *Clim Dyn* 29:73–88
- Wilks DS (1995) *Statistical methods in the atmospheric Sciences*. Academic, New york, p 467